JPET Fast Forward. Published on September 17, 2014 as DOI: 10.1124/jpet.114.217315
This article has not been copyedited and formatted. The final version may differ from this version.

Downregulation of Ca^{2+}-activated Cl^- channel TMEM16A by the inhibition of histone deacetylase in TMEM16A-expressing cancer cells

Sayo Matsuba, Satomi Niwa, Katsuhiko Muraki, Saki Kanatsuka, Yurika Nakazono, Noriyuki Hatano, Masanori Fujii, Peng Zhan, Takayoshi Suzuki, Susumu Ohya

Department of Pharmacology, Division of Pathological Sciences, Kyoto Pharmaceutical University (KPU), Kyoto 607-8414, Japan (S.M., S.N., Y.N., S.K., M.F., S.O.), Laboratory of Cellular Pharmacology, School of Pharmacy, Aichi-Gakuin University (AGU), Nagoya 464-8650, Japan (K.M., N.H.), and Graduate School of Medical Science, Kyoto Prefectural University of Medicine (KPUM), Kyoto 403-8334, Japan (P.Z., T.S.)

Running title: Downregulation of TMEM16A by HDAC3 inhibition

Address correspondence to: Susumu Ohya, Ph.D.

Department of Pharmacology, Division of Pathological Sciences, Kyoto Pharmaceutical University, 5 Misasagi-Nakauchi, Yamashina, Kyoto 607-8414, Japan

E-mail: sohya@mb.kyoto-phu.ac.jp

Number of Pages: 33

Number of Figures: 8

Number of References: 51

Number of words in Abstract: 213

Number of words in Introduction: 511

Number of words in Discussion: 1136

Abbreviations: TMEM16: transmembrane proteins with unknown function 16; **ANO:** anoctamin; **DOG1:** discovered on GIST 1; **GIST:** gastrointestinal stromal tumor; **HAT:** histone acetyltransferase; **HDAC:** histone deacetylase; **HDACi:** HDAC inhibitor; **SAHA:** suberanilohydroxamic acid; **AATB:** 4-(acetylamino)-N-[2-amino-5-(2-thienyl)phenyl]-benzamide; **T247:** N-(2-aminophenyl)-4-[1-(2-thiophen-3-ylethyl)-1H-[1], [2], [3]triazol-4-yl]benzamide; **NCT-14b**: (S)-S-7-(adamant-1-ylamino)-6-(tert-butoxycarbonyl)-7-oxoheptyl-2-methylpropanethioate; **$DiBAC_4(3)$:** bis-(1,3-dibutylbarbituric acid)trimethine oxonol; **HEPES**: 4-(2-hydroxyethyl)-1-piperazineethanesulfonic acid; **DMSO**: dimethyl sulfoxide; **REST**: repressor element 1-silencing transcription factor; **EAG-1**: *ether á go-go*-1 K^+ channel;

DBC-1: deleted in breast cancer-1; **CREB-3**: cAMP response element binding protein-3; **STAT-3**: signal transducers and activators of transcription-3; **HEK**: human embryonic kidney; **PCR**: polymerase chain reaction; **WST-1**: 2-(4-Iodophenyl)-3-(4-nitrophenyl)-5-(2,4-disulfophenyl)-2H-tetrazolium, monosodium salt; **HNSCC**: head and neck squamous cell carcinoma; **EGFR**: epidermal growth factor receptor.

Recommended section assignment: Cellular and Molecular section

JPET Fast Forward. Published on September 17, 2014 as DOI: 10.1124/jpet.114.217315
This article has not been copyedited and formatted. The final version may differ from this version.

Abstract

The Ca^{2+}-activated Cl^- channel TMEM16A (also known as ANO1 or DOG1) plays an important role in facilitating cell growth and metastasis of TMEM16A-expressing cancer cells. Histone deacetylase HDAC inhibitors (HDACis) are useful agents for cancer therapy, but, it remains unclear whether ion channels are epigenetically regulated by them. Utilizing real-time PCR, Western blot and whole-cell patch clamp assays, we found a significant decrease in TMEM16A expression and its functional activity induced by vorinostat, a pan-HDACi in TMEM16A-expressing human cancer cell lines, the prostatic cancer cell line PC-3 and the breast cancer cell line YMB-1. TMEM16A downregulation was not induced by the chemotherapy drug paclitaxel in either cell type. Pharmacological blockade of HDAC3 by 1 μM T247, a HDAC3-selective HDACi elicited a large decrease in TMEM16A expression and functional activity in both cell types, and pharmacological blockade of HDAC2 by AATB (300 nM) elicited partial inhibition of TMEM16A expression (~40 %) in both. Pharmacological blockade of HDAC1 or HDAC6 did not elicit any significant change in TMEM16A expression, respectively. In addition, siRNA-induced inhibition of HDAC3 elicited a large decrease in TMEM16A transcript in both cell types. Taken together, in malignancies with a frequent gene amplification of TMEM16A, HDAC3 inhibition is suggested to exert suppressive effects on cancer cell viability via a downregulation of TMEM16A.

Introduction

The balance of histone acetyltransferase (HAT) and HDAC activity is important in the maintenance of gene regulation (Narlikar et al., 2002). In various disease states including cancer, this balance is altered, generally leading to a decrease in gene transcription. HDAC inhibitors (HDACis) are involved in the progression of mitosis through alterations in chromatin acetylation and heat-shock protein expression (Li et al., 2013). There are currently four classes of HDACis, and some of them have been shown to possess potent anti-cancer activity. A small molecule inhibitor of class I and II HDACs, vorinostat (also known as suberanilohydroxamic acid SAHA), is approved for the treatment of cutaneous T-cell lymphoma in the USA and is also being developed for other solid tumors (Marks, 2007; Iwamoto et al., 2013). However, pan-HDACis such as vorinostat have poor selectivity and high toxicity, so selective HDACis with improved efficacy and reduced toxicity would be expected to have therapeutic activity and clinical utility in a variety of cancers.

Ion channels contribute to a variety of cancer processes, such as proliferation, apoptosis, migration and invasion, via a regulation of the resting membrane potential and intracellular Ca^{2+} signaling (Yang and Brachenbury, 2013; Lang and Stournaras, 2014; Pardo and Stühmer, 2014). Pharmacological blockade of ion channels is an attractive target to both suppress tumor growth and prevent tumor metastasis. TMEM16A (also known as ANO1 or DOG1) was identified as a pore-forming subunit of the Ca^{2+}-activated Cl^- channel, with eight putative transmenbrane domains and cytosolic N- and C-termini (Yang et al., 2008; Schroeder et al., 2008; Caputo et al., 2008) and functions as a dimer (Sheridan et al., 2011; Ohshiro et al., 2013). TMEM16A is located on chromosome 11q13, which is frequently amplified in many types of human cancer (Akervall et al., 1995; Huang et al., 2002), and plays an important role in driving the amplification of 11q13 (Komatsu et al., 2006). Overexpression of TMEM16A in human cancer is associated with the facilitation of tumor growth and migration, and

TMEM16A especially contributes to the tomorigenesis that occurs in head-and-neck squamous cell carcinoma (Ayoub et al., 2010; Duvvuri et al., 2012; Ruiz et al., 2012; Jacobsen et al., 2013). siRNA-based downregulation and pharmacological blockade of TMEM16A decrease the proliferation of breast and prostate cancer cells, so TMEM16A is an attractive therapeutic target and novel biomarker for both of these cancers (Britschgi et al., 2013; Liu et al., 2012). HDACs are also considered to be therapeutic targets for both cancers (Munster et al., 2009; Ellis et al., 2009), but it remains elusive whether TMEM16A is epigenetically regulated by HDACis in TMEM16A-expressing cancer cells.

Prostate and breast cancers are the most common types of cancer in men and women, respectively. In the present study, we examined the epigenetic regulation of TMEM16A using the pan-HDACi vorinostat in the TMEM16A-expressing human prostatic cancer cell line PC-3 and the breast cancer cell line YMB-1, demonstrating that the downregulation of TMEM16A expression/function underlies the inhibition of cell proliferation in TMEM16A-expressing cancer cells. We further identified the HDAC subtype(s) involved in TMEM16A downregulation by pharmacological HDAC blockade and siRNA-induced HDAC downregulation.

Materials and Methods

Cell culture

The prostate cancer cell lines PC-3 and LNCaP (clone FGC) were supplied from RIKEN BRC through the National Bio-Resource Project of the MEXT, Japan. The breast cancer cell lines YMB-1 (with the same DNA profile as ZR-75-1), MCF-7, Hs578T-Luc and BT-549 were supplied from Health Science Research Resources Bank (Osaka, Japan). They were maintained at 37°C, in 5% CO_2 with RPMI 1640 medium or Dulbecco's modified Eagle's medium (Wako, Osaka, Japan) containing 10% fetal bovine serum (Sigma, St. Louis, MO, USA) and penicillin (100 units/ml)-streptomycin (0.1 mg/ml) mixture (Wako).

WST-1 cell viability assay

Cell viability assay using WST-1 was performed according to Dojindo's suggested protocol (Dojindo, Kumamoto, Japan). Briefly, using a density of 4×10^5 cells/ml, cells were cultured in duplicate in 96-well plates for 0-2 days. 2 hr after addition of WST-1 reagent into each well, the absorbance was measured in Bio Rad microplate reader model 3550 (Bio Rad, Hercules, CA, USA) at a test wavelength of 450 nm, a reference wavelength of 630 nm. A pair of control and treated samples was prepared from different passage cells, and then the same protocol was repeated on another day.

RNA extraction, reverse transcription and real-time PCR

Total RNA from normal human and tumor tissues were purchased from Clontech Laboratories (Palo, CA, USA), BD Biosciences (San Jose, CA, USA) and BioChain (Hayward, CA, USA). Total RNA extraction from cell lines and reverse-transcription were performed as previously reported (Ohya et al., 2011). The resulting cDNA products were amplified with gene-specific

primers, designated using Primer Express™ software (Ver 1.5; Applied Biosystems, Foster City, CA, USA).

Quantitative, real-time PCR was performed with the use of SYBR Green chemistry on an ABI 7500 sequence detector system (Applied Biosystems) as previously reported (Ohya et al., 2013). The transcriptional expression levels were determined 24 hours after compound treatment. The following PCR primers of human origin were used for real-time PCR: TMEM16A (GenBank accession number: NM_018034, 1578-1698), 121 bp; TMEM16B (NM_020373, 2651-2778), 128 bp; histone deacetylase 1 (HDAC1) (NM_004964, 708-824), 117 bp; HDAC2 (NM_001527, 298-405), 108 bp; HDAC3 (NM_003883, 699-819), 121 bp; HDAC4 (NM_006037, 3446-3585), 140 bp; HDAC5 (NM_005474, 3339-3467), 129 bp; HDAC6 (NM_006044, 3517-3637), 121 bp; HDAC7 (NM_015401, 2313-2434, 122 bp); HDAC8 (AF245664, 598-718, 121 bp); HDAC9 (NM_058176, 2252-2374), 123 bp; HDAC10 (CU013303, 1271-1420, 150 bp); HDAC11 (NM_024827, 720-840), 121 bp. β-actin (ACTB) (NM_001101, 411-511), amplicon = 101 bp. Regression analyses of the mean values of three multiplex RT-PCRs for $\log_{10}$ diluted cDNA were used to generate standard curves. Unknown quantities relative to the standard curve for a particular set of primers were calculated, yielding transcriptional quantitation of gene products relative to the endogenous standard, ACTB. To confirm the nucleotide sequences, the amplified PCR products were sequenced with an ABI PRIZM 3100 genetic analyzer (Applied Biosystems).

Western blot analysis

Proteins from the cell lysates was prepared from PC-3 and YMB-1 cell lines as previously reported (Ohya et al., 2013). The protein expression levels were determined 48 hours after compound treatment. Equal amounts of protein (50 μg/lane) were subjected to SDS-PAGE (10 %). Blots were incubated with anti-TMEM16A (abcam, Cambridge, UK) and anti-β-actin

(Medical & Biological Laboratories (MBL), Nagoya, Japan) antibodies, then incubated with anti-rabbit and anti-mouse horseradish peroxidase-conjugated IgG (Millipore, Billerica, MA, USA), respectively. An enhanced chemiluminescence detection system (GE Healthcare Japan, Tokyo, Japan) was used for the detection of the bound antibody. The resulting images were analyzed by a LAS-3000mini device (Fujifilm, Tokyo, Japan). A pair of control and treated samples was prepared from different passage cells, and then the same protocol was repeated on another day.

Downregulation of HDACs and TMEM16A by RNA interference

Downregulation of HDACs and TMEM16A by small interfering RNA (siRNA) was performed as reported previously (Yamazaki et al., 2006). Lipofectamine RNAiMAX reagent (Invitrogen) was used for all of the siRNA transfection procedures. Commercial available siRNA oligonucleotides against human HDAC1 (sc-29343), HDAC2 (sc-29345), HDAC3 (sc-35538) and TMEM16A (sc-76686) were purchased from Santa Cruz Biotechnology (Santa Cruz, CA, USA). As a control, control siRNA (type A, Santa Cruz Biotechnology) was used. The amount of siRNA used was optimized by measuring the transfection efficacy of fluorescein-conjugated control siRNA (over 80%, as determined by flow cytometry) and determined to be a final concentration of 33 nmol/L. 24 after transfection, the expression levels of HDAC and TMEM16A transcripts were assessed by real-time PCR assay. 48 hr after transfection of TMEM16A siRNA, cell viability was measured by WST-1 assay as described above.

Whole cell patch-clamp recordings

Whole cell patch-clamp experiments were performed as reported previously (Hatano et al., 2013). The resistance of electrodes was 3–5 MΩ when they were filled with the pipette

JPET Fast Forward. Published on September 17, 2014 as DOI: 10.1124/jpet.114.217315
This article has not been copyedited and formatted. The final version may differ from this version.

solution [in mM: 110 Cs-aspartate, 30 CsCl, 1 $MgCl_2$, 10 HEPES, 10 EGTA, 2 Na_2ATP (pH 7.2 by CsOH)]. Ca^{2+} concentration was buffered by adding the appropriate amount of $CaCl_2$ determined by WINMAXC program (Stanford University, Stanford, CA, USA). Membrane currents and voltage signals were digitized with a computer using an analog-digital converter (PCI6229, National Instruments Japan). Data acquisition and analysis of whole cell currents were performed using WinWCP4.65, developed by Dr. John Dempster (University of Strathclyde, UK). The liquid junction potential between the pipette and bath solutions (−10 mV) was corrected. Cells were held at -50 mV and the currents were evoked by pipette solutions containing Ca^{2+} buffered at 1 μM. The current-voltage relationship of the activated current was determined by stepping the cell from -50 mV to potentials between -50 and +50 mV for 1 s. After depolarization, repolarization to -80 mV for 1 s elicited rapidly declining tail currents. A standard HEPES-buffered bathing solution (HEPES solution) was used, with the following composition (in mM): 137 NaCl, 10 CsCl, 5.9 KCl, 2.2 $CaCl_2$, 1.2 $MgCl_2$, 14 glucose, 10 HEPES (pH 7.4 by NaOH). All experiments were performed at 25 ± 1°C.

Statistical analysis

Statistical significance among two and multiple groups was evaluated using a paired *t*-test and Tukey's test after F test or ANOVA, respectively. A two-way ANOVA test was applied to data shown in Figure 7 and 8. Statistical significance at $p<0.05$ and $p<0.01$ is indicated in the figures. Data are presented as the means ± SEM.

Chemicals

The sources of pharmacological agents were as follows: niflumic acid (Sigma-Aldrich, Tokyo, Japan), paclitaxel (Sigma-Aldrich), bafilomycin-A (Sigma-Aldrich), WST-1 (Dojindo, Kumamoto, Japan). HDAC inhibitors (vorinostat, N-hydroxy-N'-phenyl-octanediamide;

AATB, 4-(acetylamino)-N-[2-amino-5-(2-thienyl)phenyl]-benzamide; T247, N-(2-aminophenyl)-4-[1-(2-thiophen-3-ylethyl)-1H-[1], [2], [3]triazol-4-yl]benzamide; NCT-14b,

(S)-S-7-(adamant-1-ylamino)-6-(tert-butoxycarbonyl)-7-oxoheptyl-2-methylpropanethioate were supplied from Professor Suzuki (KPUM). The others were obtained from Sigma-Aldrich or Wako Pure Chemical Industries (Tokyo, Japan).

Results

Effects of the pan-HDAC inhibitor, vorinostat on TMEM16A expression in PC-3 and YMB-1 cells

TMEM16A is an attractive therapeutic target in both prostate and breast cancer (Britschgi *et al.*, 2013; Liu *et al.*, 2012). We first performed quantitative analysis of the TMEM16A transcripts by real-time PCR assay in human prostate and breast tissues (from three different donors for each), human prostate cancer cell lines (PC-3 and LNCaP), human breast cancer cell lines (YMB-1, MCF-7, Hs578T and BT-549) and human breast tumor tissues (from three different donors) (Figs. 1A, 2A). The TMEM16A transcripts were highly expressed in the PC-3 and YMB-1 cell lines and breast tumor tissues, compared with normal tissues and the other cell lines (Figs. 1A, 2A). On the other hand, the expression levels of the TMEM16B/ANO2 transcripts were very low [less than 0.003 relative to ACTB (in arbitrary units)] in all of the cell lines and tissues examined (supplemental Figs. S1A, S1B). We next examined the effects of vorinostat (0.1-10 μM) on PC-3 and YMB-1 cell viability. 48 hr after the treatment with vehicle (DMSO), vorinostat, niflumic acid, control siRNA (siCtrl) and siTMEM16A siRNA (siTMEM16A), the relative cell viability was expressed as a ratio relative to the controls (vehicle and siCtrl). As shown in Figures 1B and 2B, vorinostat treatment (1 and 10 μM) significantly ($p<0.01$) suppressed the cell viability in both types of cells in a concentration-dependent manner. Pharmacological and siRNA-based blockade of TMEM16A by the Ca^{2+}-activated Cl^- channel inhibitor niflumic acid (100 μM) (Figs. 1C, 2C) and TMEM16A siRNA (Figs. 1D, 2D) also significantly ($p<0.01$) suppressed cell viability in both types of cells, respectively. Real-time PCR analysis showed that the transfection of TMEM16A siRNA significantly suppressed the expression level of TMEM16A transcripts in PC-3 (~85 % inhibition) and YMB-1 (~50 % inhibition). Quantitative, real-time PCR analysis

JPET Fast Forward. Published on September 17, 2014 as DOI: 10.1124/jpet.114.217315
This article has not been copyedited and formatted. The final version may differ from this version.

showed that vorinostat treatment markedly suppressed the expression levels of the TMEM16A transcripts in both cell lines in a concentration-dependent manner (Fig. 1E, 2E), without any effect on the expression level of the TMEM16B transcripts (data not shown). The expression levels of TMEM16A in arbitrary units were 0.046 ± 0.003, 0.014 ± 0.001 and 0.005 ± 0.001 in vehicle (0.1 % DMSO)-, 1 μM vorinostat- and 10 μM vorinostat-treated PC-3 cells (n=4 for each, $p<0.01$ vs. vehicle control; $p<0.05$ vs. 1 μM vorinostat-treated), respectively and 0.118 ± 0.006, 0.059 ± 0.004 and 0.021 ± 0.008 in the vehicle-, 1 μM vorinostat- and 10 μM vorinostat-treated YMB-1 cells (n=4 for each, $p<0.01$ vs. vehicle control; $p<0.05$ vs. 1 μM vorinostat-treated), respectively. Western blot analysis also showed the vorinostat (10 μM)-induced downregulation of the TMEM16A protein in the membrane protein fraction of PC-3 (Fig. 3B) and YMB-1 (Fig. 4B), in correlation with the results obtained by real-time PCR assay. After compensation of the optical density of the TMEM16A protein band signal (115 kDa) with that of the ACTB signal (45 kDa), the TMEM16A one in the vehicle control was expressed as 1.00 (Figs. 3B, 4B). The relative optical density in vorinostat (10 μM)-treated PC-3 and YMB-1 was 0.15 ± 0.02 and 0.25 ± 0.03, respectively (n=4 for each, $p<0.01$) (Figs. 3B, 4B).

Downregulation of TMEM16A by pharmacological HDAC2 and HDAC3 inhibition in PC-3 and YMB-1 cells

We next examined the molecular characteristics of the HDAC subtypes expressed in PC-3 (Fig. 1F) and YMB-1 (Fig. 2F). In PC-3 cells, the HDAC1, HDAC2 and HDAC3 isoforms were predominantly expressed, while the HDAC1, HDAC2, HDAC3 and HDAC6 isoforms were expressed in YMB-1. In human tumor breast tissues, the HDAC1, HDAC3 and HDAC6 isoforms were highly expressed compared with normal breast tissues (supplemental Figs. S1C, S1D). We therefore examined the effects of selective HDAC inhibition on the TMEM16A

JPET Fast Forward. Published on September 17, 2014 as DOI: 10.1124/jpet.114.217315
This article has not been copyedited and formatted. The final version may differ from this version.

expression level using three chemical compounds: an HDAC1 and HDAC2 selective HDACi, AATB (IC_{50}=0.007 and 0.049 μM for HDAC1 and HDAC2, respectively and IC_{50}>>10 μM for the other HDAC isoforms) (Methot et al., 2008), an HDAC3 selective HDACi, T247 (IC_{50}=0.24 μM for HDAC3, IC_{50}>>100 μM for the other HDAC isoforms) (Suzuki et al., 2013) and an HDAC6 selective HDACi, NCT-14b (IC_{50}=0.082 μM for HDAC6, IC_{50}>3.5μM for the other HDAC isoforms) (Itoh et al., 2007). The chemical structures of these compounds are shown in supplemental Figure S3A. Quantitation analyses of the protein expression levels were performed as described above. As shown in Figure 3A and 3B, 1 μM T247 exhibited a similar level of suppression of TMEM16A transcripts and proteins in PC-3 cells. On the other hand, a high concentration (300 nM) of AATB partially suppressed TMEM16A expression, while a low concentration (30 nM) of AATB or 1 μM NCT-14b did not elicit any significant change (Figs. 3A, 3B). Similar results were obtained using YMB-1 cells (Figs. 4A, 4B). The chemotherapy drugs paclitaxel and bafilomycin-A (a vacuolar-ATPase inhibitor) exhibited marked suppressive effects on cell proliferation in both of these cell lines (not shown), but no suppressive effect on TMEM16A expression was observed (Figs. 3, 4). Also, niflumic acid (100 μM) did not induce any significant decrease in TMEM16A expression in either cell type (data not shown). Treatment of T247 for 48 hrs induced the suppression of cell proliferation in both types of cells, but the suppresive effect was obviously weak compared with vorinostat (supplemental Figs. S3B, S3C). Chou et al. (2008) reported that the hydroxamates such as vorinostat have a fast acting inhibitory mechanism compared with benzamide-type HDACis, such as AATB, T247 and NCT-14b. In accord with this, vorinostat significantly ($p<0.01$) suppressed the expression of TMEM16A transcripts 12 hr after compound supplementation in both cell types, but no significant suppressive effects were observed for the other compounds in either cell type (supplemental Figs. S2B, S2D). Moreover, we examined the effects of vorinostat (1 and 10 μM) and T247 (1 μM) on the cell viability in the prostate and breast

JPET Fast Forward. Published on September 17, 2014 as DOI: 10.1124/jpet.114.217315
This article has not been copyedited and formatted. The final version may differ from this version.

cancer cell lines expressing TMEM16A less abundantly: LNCaP, MCF-7 and Hs578T. 10 μM vorinostat significantly suppressed the cell viability in LNCaP and Hs578T (supplemental Figs. S4A and S4C), however, 1 μM vorinostat and 1 μM T247 showed no significant inhibitory effects on the cell viability in LNCaP, MCF-7 and Hs578T (supplemental Fig. S4). Taken together, TMEM16A may be mostly downregulated by pharmacological blockade of HDAC3 in TMEM16A-expressing cancer cells.

The suppressive effect of HDACis on Ca^{2+}-activated Cl^- currents in PC-3 and YMB-1 cells

In PC-3 (Fig. 5) and YMB-1 (Fig. 6) cells, Ca^{2+}-activated Cl^- currents were recorded using a whole-cell configuration with a pipette solution containing Ca^{2+} fixed at 1 μM and 140 mM Cs^+. Just after membrane disruption, outwardly rectifying currents were not observed by the application of depolarizing steps (from -50 mV to +50 mV for 1 sec) in either cell type treated with vehicle (0.1 % DMSO) for 24-48 hr (data not shown), but 5-10 min after membrane disruption, application of the depolarizing steps revealed slowly activating, outwardly rectifying currents and repolarization to -80 mV for 1 sec elicited rapidly declining tail currents in the vehicle control (Figs. 5Aa, 5Ba, 6Aa and 6Ba), with voltage-dependent characteristics similar to those observed in human TMEM16A-expressing HEK293 cells (supplemental Figs. S5Cb, S5D). Figures 5C, 5D, 6C and 6D exhibited the current amplitude at the end of depolarizing pulses. Activation of the outwardly rectifying currents 5 min after the membrane disruption was not observed when measured using Ca^{2+}-free pipette solution (supplemental Figs. S5A, S5B). Ca^{2+}-activated Cl^- currents were almost completely suppressed by treatment with 10 μM vorinostat (PC-3: Figs. 5Ab, 5C, YMB-1: Figs. 6Ab, 6C). Furthermore, Ca^{2+}-activated Cl^- currents were >90 % suppressed by treatment with 1 μM T247 (PC-3: Figs. 5Bb, 5D, YMB-1: Figs. 6Bb, 6D). The activated currents were sensitive to

JPET Fast Forward. Published on September 17, 2014 as DOI: 10.1124/jpet.114.217315
This article has not been copyedited and formatted. The final version may differ from this version.

the selective TMEM16A inhibitor, T16inh-A01 (data not shown). These results are consistent with those of the expression profile experiments.

Inhibition of TMEM16 transcription by siRNA-induced HDAC3 downregulation in PC-3 and YMB-1 cells

We further examined the effect of selective HDAC1/HDAC2/HDAC3 inhibition using RNA interference. Transfection efficacy was determined using FITC-conjugated control siRNA-A in PC-3 and YMB-1 cells (over 80 %, see 'Materials and Methods'). Quantitative, real-time PCR analysis showed that HDAC3 downregulation (~75 % inhibition) markedly suppressed the expression level of the TMEM16A transcripts (~75 % inhibition) in PC-3 cells (Fig. 7C, 7D). In contrast, HDAC1 or HDAC2 downregulation did not elicit any significant ($p>0.05$) decrease in TMEM16A expression (Figs. 7A, 7B and 7D) in PC-3 cells. Similarly, in YMB-1 cells, HDAC3 (~65 % inhibition) and HDAC2 downregulation (~60 % inhibition) significantly ($p<0.01$) suppressed the expression level of the TMEM16A transcripts (~70 and 40 %, respectively) (Figs. 8B, 8C and 8D). On the other hand, HDAC1 downregulation did not exert any significant ($p>0.05$) suppressive effect on TMEM16A expression (Figs. 8A, 8D). Control siRNA did not exert any significant effects on HDAC1-3 and TMEM16A expression. The expression levels of TMEM16A (in arbitrary units) were 0.040 ± 0.003, 0.042 ± 0.006 and 0.013 ± 0.003 in HDAC1-, HDAC2- and HDAC3-downregulated PC-3 cells, respectively. The expression levels of TMEM16A (in arbitrary units) were 0.095 ± 0.006, 0.062 ± 0.004 and 0.027 ± 0.003 in HDAC1-, HDAC2-, and HDAC3-downregulated YMB-1 cells, respectively. These suggest that HDAC3 is the leading candidate for TMEM16A suppression.

JPET Fast Forward. Published on September 17, 2014 as DOI: 10.1124/jpet.114.217315
This article has not been copyedited and formatted. The final version may differ from this version.

Discussion

In cancer cells, ion channels regulate cell proliferation and apoptosis via the modulation of membrane potential and intracellular Ca^{2+}-mobilization (Yang and Brachenbury, 2013; Lang and Stournaras, 2014; Pardo and Stühmer, 2014), and thus are both potential therapeutic targets and biomarkers for cancer. Histone acetylation and DNA methylation on gene expression play important roles in various cellular processes such as proliferation, differentiation and apoptosis, and DNA methylation is a key regulator of the transient receptor potential Ca^{2+} channel TRPC3 and inward-rectifier K^+ channel $K_{ir}4.1$ (Martin-Trujillo et al., 2011; Nwaobi et al., 2014). Epigenetic modification-based therapy with HDACis is one of the novel strategies for cancer treatment. However, the role of HDAC in the ion channel regulatory effect of HDACis on ion channel expression is less clear. Recently, it was reported that the Ca^{2+}-activated Cl^- channel TMEM16A is a potential therapeutic target and biomarker for prostate and breast cancers as well as head and neck squamous cell carcinomas (HNSCCs) (Britschgi et al., 2013; Liu et al., 2012; Ayoub et al., 2010). Britschgi et al. (2013) showed that a reduction in epidermal growth factor receptor (EGFR) signaling by TMEM16A knockdown is strongly associated with a decrease in breast cancer cell viability.

The main findings in the present study are as follows. 1) Epigenetic modulation of the Ca^{2+}-activated Cl^- channel TMEM16A by the clinically available pan-HDACi vorinostat in TMEM16A-expressing cancer cell lines, i.e. the prostate cancer cell line PC-3 and the breast cancer cell line YMB-1. 2) The identification of HDAC subtypes related to epigenetic regulation of TMEM16A by pharmacological and siRNA-mediated inhibition of HDACs. The chemotherapy drugs paclitaxel and bafilomycin-A exhibit antiproliferative effects (data not shown) without any significant effect on the TMEM16A expression levels in PC-3 and YMB-1 cells (Fig. 3, 4). Our results suggest that HDAC3 plays a crucial role in the epigenetic regulation of TMEM16A in TMEM16A-expressing cancer cells.

JPET Fast Forward. Published on September 17, 2014 as DOI: 10.1124/jpet.114.217315
This article has not been copyedited and formatted. The final version may differ from this version.

HDAC3 transcripts were highly expressed in PC-3, YMB-1 and human tumor breast tissues (Figs. 1F, 2F, supplemental Fig. S1D). Pharmacological and siRNA-mediated HDAC3 inhibition caused marked downregulation of TMEM16A expression in PC-3 and YMB-1 cells (Figs. 3, 4, 7 and 8), and its functional activity is essentially disappeared as a result of treatment with the selective HDAC3 inhibitor T247 (1 μM) for 24-48 hr in both cell types (Figs. 5, 6). In correspondance with these results, cell viability in both cell types were significantly ($p<0.05$ or 0.01) inhibited by the treatment with T247 (1 μM), niflumic acid (100 μM) and TMEM16A siRNA, respectively (supplemental Figs. S3B, S3C; Figs. 1C, 1D, 2C, 2D). Pharmacological HDAC2 blockade in both types of cells or siRNA-mediated HDAC2 inhibition in YMB-1 alone caused ~30 % inhibition of the TMEM16A expression (Figs. 4, 8D), but it did not exhibit any significant effect on cell viability (supplemental Figs. S3B, S3C). Significant inhibition of cell viability was observed by the treatment with 100 μM niflmic acid (Figs. 1C, 2C) in both types of cells, but the treatment with 10 μM niflumic acid did not induce any changes (<5 % in both) in cell viability (data not shown). These suggest that the significant suppression of signaling pathways that control cell proliferation (i.e. EGFR signaling) may not be induced by partial inhibition of TMEM16A activity in both types of cells. Recently, it has been reported that HDAC3 inhibition causes a decrease in proliferation and/or migration in breast cancer cells (Kim et al., 2010; Müller et al., 2013), and HDAC3 is strongly expressed in breast cancer of a more aggressive tumor type (Müller et al., 2013) . Our previous study showed that human prostate cancer progression may be linked to the changes in the expression levels of Ca^{2+}-activated K^+ channel subtypes $K_{Ca}1.1$ and $K_{Ca}3.1$ (Ohya et al., 2009). Britschgi et al. (2013) have shown that amplification of TMEM16A correlates with both disease severity and poor prognosis in human breast cancer. It remains unclear whether amplification of HDAC3 correlates with disease severity and prognosis in breast cancer, but in gliomas, a high level of HDAC3 expression correlates with

JPET Fast Forward. Published on September 17, 2014 as DOI: 10.1124/jpet.114.217315
This article has not been copyedited and formatted. The final version may differ from this version.

a high tumor grade (Zhu et al., 2013). Taken together, the dysfunction of TMEM16A induced by HDAC3 inhibition is at least in part responsible for the decrease in cell viability in PC-3 and YMB-1 cells, and it may be related to the comparatively poor migration and invasion capacity observed in TMEM16A-overexpressing metastatic cancer cells.

One of the mechanisms underlying HDAC-induced promotion of tumor onset and progression is the repression of tumor suppressor gene transcription (Ropero and Esteller, 2007). Due to the epigenetic modification, HDACis are able to upregulate tumor suppressor gene expression, resulting in inhibited cancer cell viability (Gui et al., 2004). For example, several HDACis upregulate the tumor suppressor p53 (Kim et al., 2001) and the repressor element 1-silencing transcription factor REST (also called 'neuron-restrictive silencer factor, NRSF') (Taylor et al., 2012) in cancer cells. These suppressors play important roles in repressing ion channel expression. Indeed, p53 negatively regulates the voltage-gated K^+ channel EAG1 (Lin et al., 2011), while REST negatively regulates the voltage-gated K^+ channel $K_V4.3$ and Ca^{2+}-activated K^+ channel $K_{Ca}3.1$ in several different types of cells including cancer cells (Cheong et al., 2005; Uchida et al., 2010; Ohya et al., 2011). HDAC3 selectively binds to many types of transcriptional repressors. For example, HDAC3 represses the following tumor suppressors: DBC-1 (deleted in breast cancer-1) (Chini et al., 2010), CREB-3 (cAMP response element binding protein-3) (Kim et al., 2010) and STAT-3 (signal transducers and activators of transcription-3) (Minami et al., 2014; Miao et al., 2014) in various types of cancer cells, including breast cancer cells. The molecular mechanism(s) underlying the epigenetic modulation of TMEM16A transcription remains to be elucidated, so further studies (e.g. genetic structure and promoter analysis of TMEM16A and siRNA-mediated knockdown of HDAC3-related tumor suppressors) will be needed to clarify the pathophysiological significance of epigenetic modulation of TMEM16A in TMEM16A-expressing cancer cells.

JPET Fast Forward. Published on September 17, 2014 as DOI: 10.1124/jpet.114.217315
This article has not been copyedited and formatted. The final version may differ from this version.

In conclusion, this study provides the novel evidence that the Ca^{2+}-activated Cl^- channel TMEM16A is epigenetically-regulated by the inhibition of histone deacetylases in TMEM16A-expressing cancer cells. Of note, TMEM16A transcription in the respective prostate and breast cancer cell lines PC-3 and YMB-1 is mostly regulated by HDAC3. Pharmacological and siRNA-mediated inhibition of HDAC3 inhibited TMEM16A expression and interfered with cell viability. TMEM16A is known to be overexpressed and to regulate migration and invasion of metastatic cancer cells. Therefore, these findings constitute important information for an epigenetic modification-based therapeutic strategy by HDACis in metastatic prostate and breast cancers. In addition, TMEM16A is involved in a variety of biological functions, such as epithelial secretion, neuronal excitability, nociception and gastrointestinal motility (Duran and Hartzell, 2013). Recent studies have shown that HDAC3 is involved in neurodegenerative, gastrointestinal and inflammatory diseases (Chen et al., 2012; Alenghat et al., 2013; Venkatraman et al., 2014). Therefore, TMEM16A inhibition via pharmacologic blockade of HDAC3 may have a therapeutic potential for wide range of disorders.

Acknowledgements

We thank to Masuno Y (KPU), Matsui A (KPU) and Yotsutsuji K (AGU) for their technical assistance. Pacific Edit (San Francisco, USA) reviewed the manuscript prior to submission.

Disclosures

No conflicts of interest, financial or otherwise are declared by the authors.

Authorship Contributions

Participated in research design: Ohya, Muraki, Suzuki

Conducted experiments: Matsuba, Niwa, Kanatsuka, Nakazono, Ohya, Muraki, Hatano, Zhan

Performed data analysis: Matsuba, Niwa, Kanatsuka, Nakazono, Ohya, Muraki, Hatano, Fujii

Wrote or contributed to the writing of the manuscript: Ohya, Matsuba, Niwa, Muraki, Hatano, Suzuki

References

Akervall JA, Jin Y, Wennerberg JP, Zätterström UK, Kjellén E, Mertens F, Willén R, Mandahl N, Heim S, and Mitelman F (1995) Chromosomal abnormalities involving 11q13 are associated with poor prognosis in patients with squamous cell carcinoma of the head and neck. *Cancer* **76**: 853-859.

Alenghat T, Osborne LC, Saenz SA, Kobuley D, Ziegler CG, Mullican SE, Choi I, Grunberg S, Sinha R, Wynosky-Dolfi M, Snyder A, Giacomin PR, Joyce KL, Hoang TB, Bewtra M, Brodsky IE, Sonnenberg GF, Bushman FD, Won KJ, Lazar MA, Artis D (2013) Histon deacetylase 3 coordinates commensal-bacteria-dependent intestinal homeostasis. *Nature (Lond)* **504**: 153-157.

Ayoub C, Wasylyk C, Li Y, Thomas E, Marisa L, Robé A, Roux M, Abecassis J, and de Reyniès A, Wasylyk B (2010) ANO1 amplification and expression in HNSCC with a high propensity for future distant metastasis and its dunctions in HNSCC cell lines. *Br J Cancer* **103**: 714-726.

Britschgi A, Bill A, Brinkhaus H, Rothwell C, Clay I, Duss S, Rebhan M, Raman P, Guy CT, Wetzel K, George E, Popa MO, Liley S, Choudhury H, Gosling M, Wang L, Fitzgerald S, Borawski J, Baffoe J, Labow M, Gaither LA, and Bentires-Alj M (2013) Calcium-activated chloride channel ANO1 promotes breast cancer progression by activating EGFR and CAMK signaling. *Proc Natl Acad Sci U S A* **110**: E1026-E1034.

Caputo A, Caci E, Ferrera L, Pedemonte N, Barsanti C, Sondo E, Pfeffer U, Ravazzolo R, Zegarra-Moran O, and Galietta LJ (2008) TMEM16A, a member protein associated with calcium-dependent chloride channel activity. *Science* **322**: 590-594.

Chen X, Barozzi I, Termanini A, Prosperini E, Recchiuti A, Dalli J, Mietton F, Matteoli G, Hiebert S, Natoli G (2012) Requirement for the histone deacetylase Hdac3 for the

inflammatory gene expression program in macrophages. *Proc Natl Acad Sci U S A* **109**: E2865-E2874.

Cheong A, Bingham AJ, Li J, Kumar B, Sukumar P, Munsch C, Buckley NJ, Neylon CB, Porter KE, Beech DJ, and Wood IC (2005) Downregulated REST transcription factor is a switch enabling critical potassium channel expression and cell proliferation. *Mol Cell* **20**: 45-52.

Chini CCS, Escande C, Nin V, Chini EN (2010) HDAC3 is negatively regulated by the nuclear protein DBC. *J Biol Chem* **285**: 40830-40837.

Chou CJ, Herman D, and Gottesfeld JM (2008) Pimelic diphenylamide 106 is a slow, tight-binding inhibitor of class I histone deacetylases. *J Biol Chem* **283**: 35402-35409.

Duan C, and Hartzell C (2011) Physiological roles and diseases of Tmem16 / anoctamin proteins: Are they all chrolide channels? *Acta Pharmacol Sin* **32**: 685-692.

Duvvuri U, Shiwarski DJ, Xiao D, Bertrand C, Huang X, Edinger RS, Rock JR, Harfe BD, Henson BJ, Kunzelmann K, Schreiber R, Seethala RS, Egloff AM, Chen X, Lui VW, Grandis JR, and Gollin SM (2012) TMEM16A induces MAPK and contributes directly to tumorigenesis and cancer progression. *Cancer Res* **72**: 3270-3281.

Ellis L, Hammers HJ, and Pili R (2009) Targeting tumor angiogenesis with histone deacetylase inhibitors. *Cancer Lett* **280**: 145-153.

Gui C-Y, Ngo L, Xu WS, Richon VM, and Marks PA (2004) Histone deacetylase (HDAC) inhibitor activation of $p21^{WAF1}$ involves changes in promoter-associated proteins, including HDAC1. *Proc Natl Acad Sci U S A* **101**: 1241-1246.

Hatano N, Suzuki H, Muraki Y, and Muraki K (2013) Stimulation of human TRPA1 channels by clinical concentrations of the antirheumatic drug auranofin. *Am J Physiol Cell Physiol* **304**: C354-C361.

Huang X, Gollin SM, Raja S, and Godfrey TE (2002) High-resolution mapping of the 11q13 amplicon and identification of a gene, TAOS1, that is amplified and over expressed in oral cancer cells. *Proc Natl Acad Sci U S A* **99**: 11369-11374.

Itoh Y, Suzuki T, Kouketsu A, Suzuki N, Maeda S, Yoshida M, Nakagawa H, and Miyata N (2007) Design, synthesis, structure-selectivity relationship, and effect on human cancer calls of a novel series of histone deacetylase 6-selective inhibitors. *J Med Chem* **50**: 5425-5438.

Iwamoto M, Friedman EJ, Sandhu P, Agrawal NG, Rubin EH, and Wagner JA (2013) Clinical pharmacology profile of vorinostat, a histone deacetylase inhibitor. *Cancer Chemothr Pharmacol* **72**: 493-508.

Jacobsen KS, Zeeberg K, Sauter DR, Poulsen KA, Hoffmann EK, and Schwab A (2013) The role of TMEM16A (ANO1) and TMEM16F (ANO6) in cell migration. *Pflügers Arch* **465**: 1753-1762.

Kim HC, Choi KC, Choi HK, Kang HB, Kim MJ, Lee YH, Lee OH, Lee J, Kim YJ, Jun W, Jeong JW, Yoon HG (2010) HDAC3 selectively represses CREB3-mediated transcription and migration of metastatic breast cancer cells. *Cell Mol Life Sci* **67**: 3499-3510.

Kim MS, Kwon HJ, Lee YM, Baek JH, Jang JE, Lee SW, Moon EJ, Kim HS, Lee SK, Chung HY, Kim CW, and Kim KW (2001) Histone deacetylases induce angiogenesis by negative regulation of tumor suppressor genes. *Nat Med* **7**: 437-443.

Komatsu Y, Hibi K, Kodera Y, Akiyama S, Ito K, and Nakao A (2006) TAOS1, a novel marker for advanced esophageal squamous cell carcinoma. *Anticancer Res* **26**: 2029-2032.

Lang F and Stournaras C (2014) Ion channels in cancer: future perspectives and clinical potential. *Philos Trans R Soc Lond B Biol Sci* **369**: 20130108.

Li J, Li G, and Xu W (2013) Histon deacetylase inhibitors: an attractive strategy for cancer therapy. *Curr Med Chem* **20**: 1858-1886.

Lin H, Li Z, Chen C, Luo X, Xiao J, Dong D, Lu Y, Yang B, and Wang Z (2011) Transcriptional and post-transcriptional mechanisms for oncogenic overexpression of ether à go-go K^+ channel. *PLoS ONE* **6**: e20362.

Liu W, Lu M, Liu B, Huang Y, and Wang K (2012) Inhibition of Ca^{2+}-activated Cl^- channel ANO1/TMEM16A expression suppresses tumor growth and invasiveness in human prostate carcinoma, *Cancer Lett* **326**: 41-51.

Marks PA (2007) Descovery and development of SAHA as an anticancer agent. *Oncogene* **26**: 1351-1356.

Martin-Trujillo A, Iglesias-Palatas I, Coto E, Corral-Juan M, San Nicolás H, Corral J, Volpini V, Matilla-Dueñas A, and Monk D (2011) Genotype of an individual single nucleotide polymorphism regulates DNA methylation at the TRPC3 alternative promoter. *Epigenetics* **6**: 1236-1241.

Methot JL, Chalravarty PK, Chenard M, Close J, Cruz JC, Dahlberg WK, Fleming J, Hamblett CL, Hamill JE, Harrington P, Harsch A, Heidebrecht R, Hughes B, Jung J, Kenific CM, Kral AM, Meinke PT, Middleton RE, Ozerova N, Sloman DL, Stanton MG, Szewczak AA, Tyagarajan S, Witter DJ, Secrist JP, and Miller TA (2008) Exploration of the internal cavity of histone deacetylase (HDAC) with selective HDAC1/HDAC2 inhibitors (SHI-1:2). *Bioorg Med Chem Lett* **18**: 973-978.

Miao LJ, Huang FX, Sun ZT, Zhang RX, Huang SF, Wang J (2014) Stat3 inhibits Beclin 1 expression through recruitment of HDAC3 in nonsmall cell lung cancer cells. *Tumour Biol*, in press.

Minami J, Suzuki R, Mazitschek R, Gorgun G, Ghosh B, Cirstea D, Hu Y, Mimura N, Ohguchi H, Cottini F, Jakubikova J, Munshi NC, Haggarty SJ, Richardson PG, Hideshima T, Anderson KC (2014) Histone deacetylase 3 as a novel therapeutic target in multiple myeloma. Leukemia 28: 680-689.

Müller BM, Jana L, Kasajima A, Lehmann A, Prinzler J, Budczies J, Winzer KJ, Dietel M, Weichert W, Denkert C (2013) Differential expression of histone deacetylases HDAC1, 2 and 3 in human breast cancer-overexpression of HDAC2 and HDAC3 is associated with clinicopathological indicators of disease progression. *BMC Cancer* **13**: 215.

Munster PN, Marchion D, Thomas S, Egorin M, Minton S, Springett G, Lee JH, Simon G, Chiappori A, Sullivan D, Daud A (2009) Phase I trial of vorinostat and doxorubicin in solid tumours: histone deacetylase 2 expression as a predictive marker. *Br J Cancer* **101**: 1044-1050.

Narlikar GJ, Fan HY, and Kingston RE (2002) Cooperation between complexes that regulate chromatin structure and transcription. *Cell* **108**: 475-487 (2002).

Nwaobi SE, Lin E, Peramsetty SR, and Olsen ML (2014) DNA methylation functions as a critical regulator of Kir4.1 expression during CNS development. *Glia* **62**: 411-427.

Ohshiro J, Yamamura H, Saeki T, Suzuki Y, and Imaizumi Y (2014) The multiple expression of Ca^{2+}-activated Cl^- channels via homo- and hetero-dimer formation of TMEM16A splicing variants in murine portal vein. *Biochem Biophys Res Commun* **443**: 518-523.

Ohya S, Kimura K, Niwa S, Ohno A, Kojima Y, Sasaki S, Kohri K, and Imaizumi Y (2009) Malignancy grade-dependent expression of K^+-channel subtypes in human prostate cancer. *J Pharmacol Sci* **109**: 148-151.

Ohya S, Nakamura E, Horiba S, Kito H, Matsui M, Yamamura H, and Imaizumi Y (2013) Role of the $K_{Ca}3.1$ K^+ channel in auricular lymph node T-lymphocyte function of the delayed-type hypersensitivity model. *Br J Pharmacol* **169**: 1011-1023.

Ohya S, Niwa S, Kojima Y, Sasaki S, Sakuragi M, Kohri K, and Imaizumi Y (2011) Intermediate-conductance Ca^{2+}-activated K^+ channel, $K_{Ca}3.1$, as a novel therapeutic target for benign prostatic hyperplasia. *J Pharmacol Exp Ther* **338**: 528-536.

Pardo LA and Stühmer W (2014) The roles of K^+ channels in cancer. *Nat Rev Cancer* **14**: 39-48.

Ropero S and Esteller M (2007) The role of histone deacetylases (HDACs) in human cancer. *Mol Oncol* **1**: 19-25.

Ruiz C, Martins JR, Rudin F, Schneider S, Dietsche T, Fischer CA, Tornillo L, Terracciano LM, Schreiber R, Bubendorf L, and Kunzelmann K (2012) Enhanced expression of ANO1 in head and neck squamous cell carcinoma causes cell migration and correlates with poor prognosis. *PLoS One* **7**: e43265.

Schroeder BC, Cheng T, Jan YN, and Jan LY (2008) Expression cloning of TMEM16A as a calcium-activated chloride channel subunit. *Cell* **134**: 1019-1029.

Sheridan JT, Worthington EN, Yu K, Gabriel SE, Hartzell HC, and Tarran R (2011) Characterization of the oligomeric structure of the Ca^{2+}-activated Cl^- channel Ano1/TMEM16A. *J Biol Chem* **286**: 1381-1388.

Suzuki T, Kasuya Y, Itoh Y, Ota Y, Zhan P, Asamitsu K, Nakagawa H, Okamoto T, and Miyata N (2013) Identification of highly selective and potent histone deacetylase 3 inhibitors using click chemistry-based combinatiorial fragment assembly. *PLoS One* **8**: e68669.

Taylor P, Fangusaro J, Rajaram V, Goldman S, Helenowski IB, MacDonald T, Hasselblatt M, Riedemann L, Laureano A, Cooper L, and Gopalakrishnan V (2012) REST is a novel prognostic factor and therapeutic target for medullpblastoma. *Mol Cancer Ther* **11**: 1713-1723.

Uchida H, Sasaki K, Ma L, and Ueda H (2010) Neuron-restrictive silencer factor causes epigenetic silencing of Kv4.3 gene after peripheral nerve injury. *Neuroscience* **166**: 1-4.

Venkatraman A, Hu YS, Didonna A, Cvetanovic M, Krbanjevic A, Bilesimo P, Opal P (2014) The histone deacetylase HDAC3 is essential for Purkinje cell function, potentially

complicating the use of HDAC inhibitors in SCA1. *Hum Mol Genet* doi: 10.1093/hmg/ddu081.

Yamazaki D, Aoyama M, Ohya S, Muraki K, Asai K, and Imaizumi Y (2006) Novel functions of small conductance Ca^{2+}-activated K^{+} channel in enhanced cell proliferation by ATP in brain endothelial cells. *J Biol Chem* **281**: 38430-38439.

Yang M and Brachenbury WJ (2013) Membrane potential and cancer progression. *Front Physiol* **4**:185.

Yang YD, Cho H, Koo JY, Tak MH, Cho Y, Shim WS, Park SP, Lee J, Lee B, Kim BM, Raouf R, Shin YK, and Oh U (2008) TMEM16A confers receptor-activated calcium-dependent chloride conductance. *Nature (Lond)* **455**: 1210-1215.

Zhu J, Wan H, Xue C, jiang T, Qian C, and Zhang Y (2013) Histone deacetylasse 3 implicated in the pathogenesis of children glioma by promoting glioma cell proliferation and migration. *Brain Res* **1520**: 15-22.

Footnotes

This work was supported by a Grant-in-Aid for Scientific Research (C) from the Japan Society for the Promotion of Science (JSPS) (No. 25460111), a research grant from The Promotion and Mutual Aid Cooperation for Private Schools of Japan (Kyoto Pharmaceutical Univ and Aichi-Gakuin Univ.), Mochida Memorial Foundation for Medical and Pharmaceutical Research and Uehara Memorial Foundation (S.O.).

Figure legends

Figure 1. Effects of vorinostat on cell viability and TMEM16A transcript expression in PC-3 cells. A: Quantitative, real-time PCR assay for TMEM16A in human normal prostate tissues and human prostate cancer cell lines (PC-3 and LNCaP). B, C, D: Effects of vorinostat (0.1, 1.0 and 10 μM) (B), niflumic acid (100 μM) (C) and TMEM16A siRNA (D) on cell viability in PC-3 cells. E: Effects of vorinostat (1.0 and 10 μM) on the expression level of TMEM16A transcripts in PC-3 cells. F: Gene expression profiling of the 11 HDAC isoforms in PC-3 cells. The expression levels were expressed as the ratio to β-actin (ACTB). The results are expressed as the means ± SEM. The numbers used for the experiments are shown in parentheses. **: $p<0.01$ vs. vehicle control, #: $p<0.05$ vs. 1 μM vorinostat treatment.

Figure 2. Effects of vorinostat on cell viability and TMEM16A transcript expression in YMB-1 cells. A: Quantitative, real-time PCR assay for TMEM16A in human normal and tumor breast tissues and human breast cancer cell lines (YMB-1, MCF-7, Hs578T and BT-549). B, C, D: Effects of vorinostat (0.1, 1.0 and 10 μM) (B), niflumic acid (100 μM) (C) and TMEM16A siRNA (D) on cell viability in YMB-1 cells. E: Effects of vorinostat (1.0 and 10 μM) on the expression level of TMEM16A transcripts in YMB-1 cells. F: Gene expression profiling of the 11 HDAC isoforms in YMB-1 cells. The expression levels were expressed as the ratio to ACTB. The results are expressed as the means ± SEM. The numbers used for the experiments are shown in parentheses. **: $p<0.01$ vs. vehicle control, #: $p<0.05$ vs. 1 μM vorinostat treatment.

Figure 3. Effects of selective HDACis and chemotherapy drugs on the expression levels of TMEM16A transcript and protein levels in PC-3 cells. A: Real-time PCR assay for TMEM16A in PC-3 cells. Effects of AATB (30 nM, selective for HDAC1; 300 nM, selective

for HDAC2), T247 (1 μM, selective for HDAC3), NCT-14b (1 μM, selective for HDAC6), paclitaxel (100 nM) and bafilomycin-A (10 nM) on the transcriptional expression of TMEM16A. The expression levels were expressed as the ratio to ACTB. B: Proteins from the cell lysates of PC-3 cells were probed by immunoblotting with anti-TMEM16A/ANO1 and anti-ACTB antibodies. Effects of AATB (300 nM), T247 (1 μM), NCT-14b (1 μM) and paclitaxel (100 nM) on the protein expression of TMEM16A. The arrowheads indicate the migrating positions of TMEM16A (115 kDa) and ACTB (45 kDa). The summarized results were obtained as the optical density of TMEM16A and ACTB band signals in the compound treated-groups relative to that in vehicle control. The results are expressed as the means ± SEM (n=4 for each in A and B). *,**: $p<0.05$, 0.01 vs. vehicle control.

Figure 4. Effects of selective HDACis and chemotherapy drugs on the expression levels of TMEM16A transcript and protein levels in YMB-1 cells. A: Real-time PCR assay for TMEM16A in YMB-1 cells. Effects of AATB (30 nM, selective for HDAC1; 300 nM, selective for HDAC2), T247 (1 μM, selective for HDAC3), NCT-14b (1 μM, selective for HDAC6), paclitaxel (100 nM) and bafilomycin-A (10 nM) on the transcriptional expression of TMEM16A. The expression levels were expressed as the ratio to ACTB. B: Proteins from the cell lysates of YMB-1 cells were probed by immunoblotting with anti-TMEM16A/ANO1 and anti-ACTB antibodies. Effects of AATB (300 nM), T247 (1 μM), NCT-14b (1 μM) and paclitaxel (100 nM) on the protein expression of TMEM16A. The arrowheads indicate the migrating positions of TMEM16A (115 kDa) and ACTB (45 kDa). The summarized results were obtained as the optical density of TMEM16A and ACTB band signals in the compound treated-groups relative to that in vehicle control. The results are expressed as the means ± SEM (n=4 for each in A and B). *,**: $p<0.05$, 0.01 vs. vehicle control.

Figure 5. Effects of treatment with vorinostat (10 μM) and T247 (1 μM) on Ca^{2+}-activated Cl^- currents in PC-3 cells. A, B: Ca^{2+}-activated Cl^- currents were recorded using a whole-cell configuration with a pipette solution containing mostly 1 μM Ca^{2+} and 140 mM Cs^+. 5-10 min after membrane disruption, the slowly activating, outwardly rectifying currents induced by the application of depolarizing steps (from -50 to +50 mV for 1 sec) and rapidly declining tail currents by the application of repolarization to -80 mV for 1 sec were observed in vehicle control (Aa, Ba). 30-48 hrs after treatment with vorinostat (10 μM) (Ab) and T247 (1 μM) (Bb), Ca^{2+}-activated Cl^- currents were almost disappeared. C, D: Current-voltage relationship for the current amplitude at the end of depolarization pulse (at +50 mV) in vorinostat-treated (C) and T247-treated (D) groups. The numbers used for the experiments are shown in parentheses. The results are expressed as the means ± SEM. **: $p<0.01$ vs. vehicle control.

Figure 6. Effects of treatment with vorinostat (10 μM) and T247 (1 μM) on Ca^{2+}-activated Cl^- currents in YMB-1 cells. A, B: Ca^{2+}-activated Cl^- currents were recorded using a whole-cell configuration with a pipette solution containing mostly 1 μM Ca^{2+} and 140 mM Cs^+. 5-10 min after membrane disruption, the slowly activating, outwardly rectifying currents induced by the application of depolarizing steps (from -50 to +50 mV for 1 sec) and rapidly declining tail currents by the application of repolarization to -80 mV for 1 sec were observed in vehicle control (Aa, Ba). 30-48 hrs after treatment with vorinostat (10 μM) (Ab) and T247 (1 μM) (Bb), Ca^{2+}-activated Cl^- currents were almost disappeared. C, D: Current-voltage relationship for the current amplitude at the end of depolarization pulse (at +50 mV) in vorinostat-treated (C) and T247-treated (D) groups. The numbers used for the experiments are shown in parentheses. The results are expressed as the means ± SEM. **: $p<0.01$ vs. vehicle control.

Figure 7. Effects of siRNA-mediated HDAC inhibition on HDAC1-3 and TMEM16A

transcription in PC-3 cells. A-C: Inhibition of the HDAC1 (A), HDAC2 (B) and HDAC3 (C) transcription by siRNAs specific for the HDAC subtypes: siCtrl, siRNA for control siRNA-A; siHDAC1, siRNA for HDAC1; siHDAC2, siRNA for HDAC2; siHDAC3, siRNA for HDAC3. D: Effects of siCtrl and siHDAC1-3 on the transcriptional expression level of TMEM16A in PC-3 cells. The results are expressed as the means ± SEM (n=4 for each) **: $p<0.01$ vs. siCtrl.

Figure 8. Effects of siRNA-mediated HDAC inhibition on HDAC1-3 and TMEM16A transcription in YMB-1 cells. A-C: Inhibition of the HDAC1 (A), HDAC2 (B) and HDAC3 (C) transcription by siRNAs specific for the HDAC subtypes: siCtrl, siRNA for control siRNA-A; siHDAC1, siRNA for HDAC1; siHDAC2, siRNA for HDAC2; siHDAC3, siRNA for HDAC3. D: Effects of siCtrl and siHDAC1-3 on the transcriptional expression level of TMEM16A in YMB-1 cells. The results are expressed as the means ± SEM (n=4 for each) **: $p<0.01$ vs. siCtrl.

JPET Fast Forward. Published on September 17, 2014 as DOI: 10.1124/jpet.114.217315
This article has not been copyedited and formatted. The final version may differ from this version.

Fig. 1

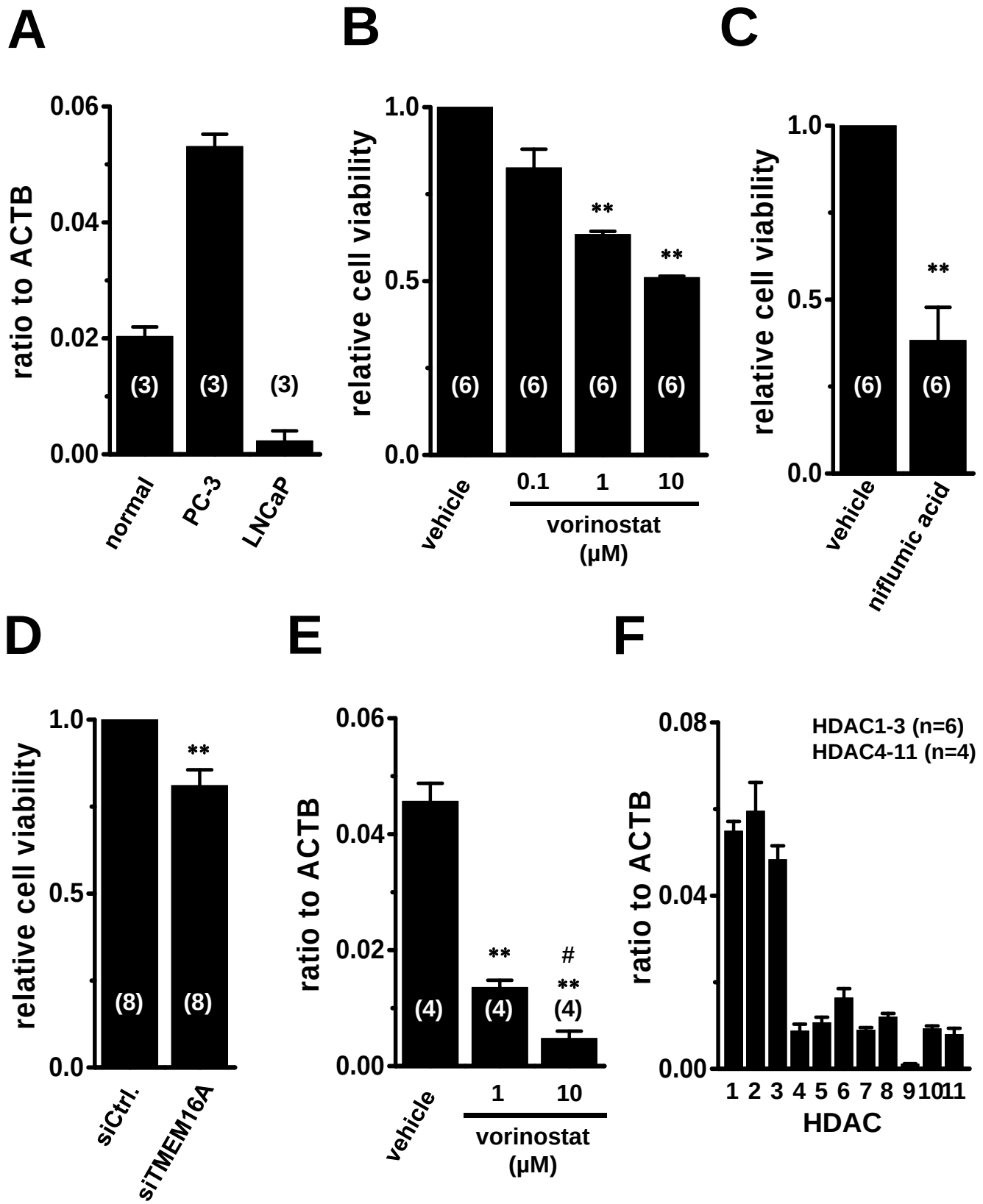

JPET Fast Forward. Published on September 17, 2014 as DOI: 10.1124/jpet.114.217315
This article has not been copyedited and formatted. The final version may differ from this version.

Fig. 2

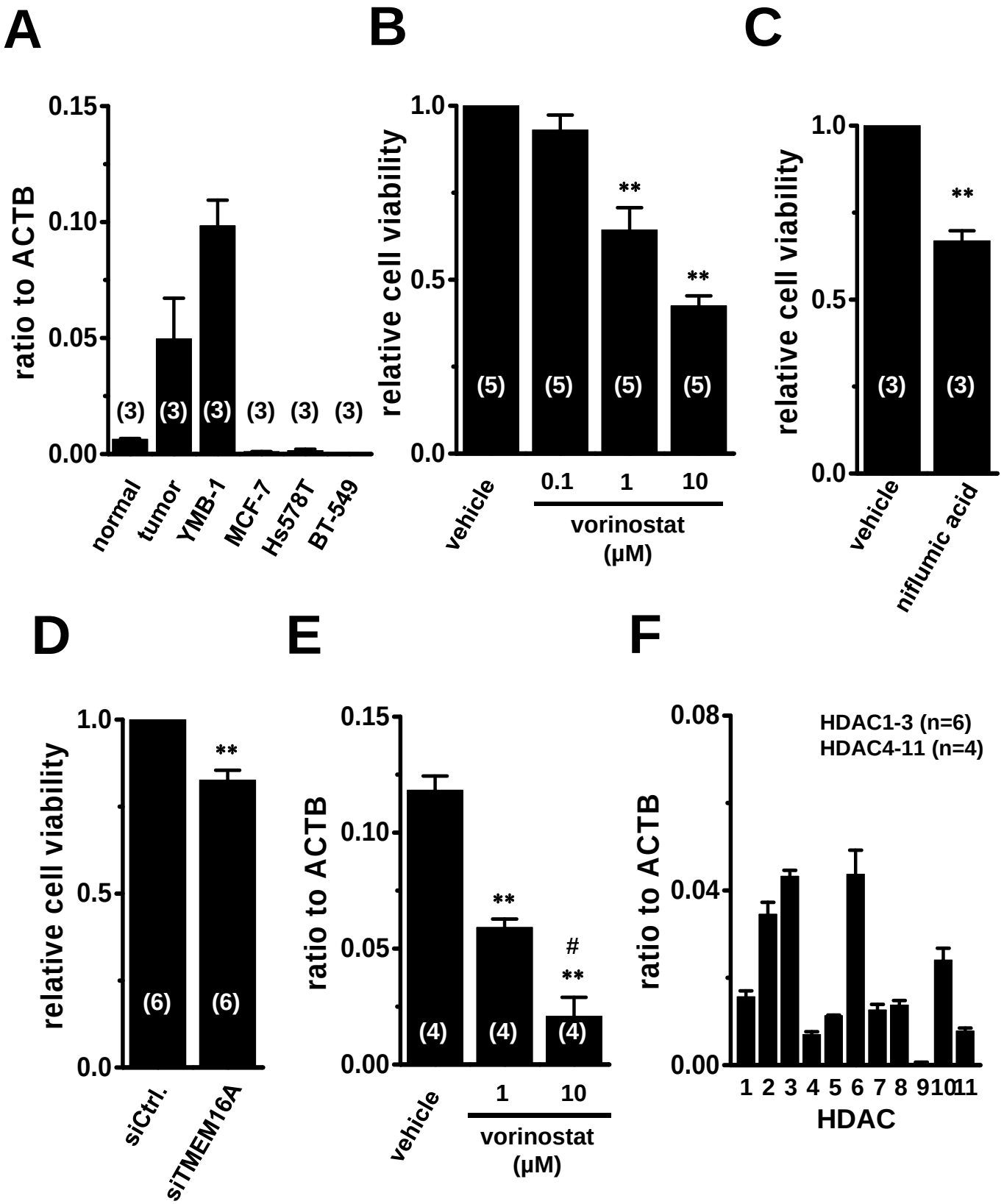

JPET Fast Forward. Published on September 17, 2014 as DOI: 10.1124/jpet.114.217315

Fig. 3

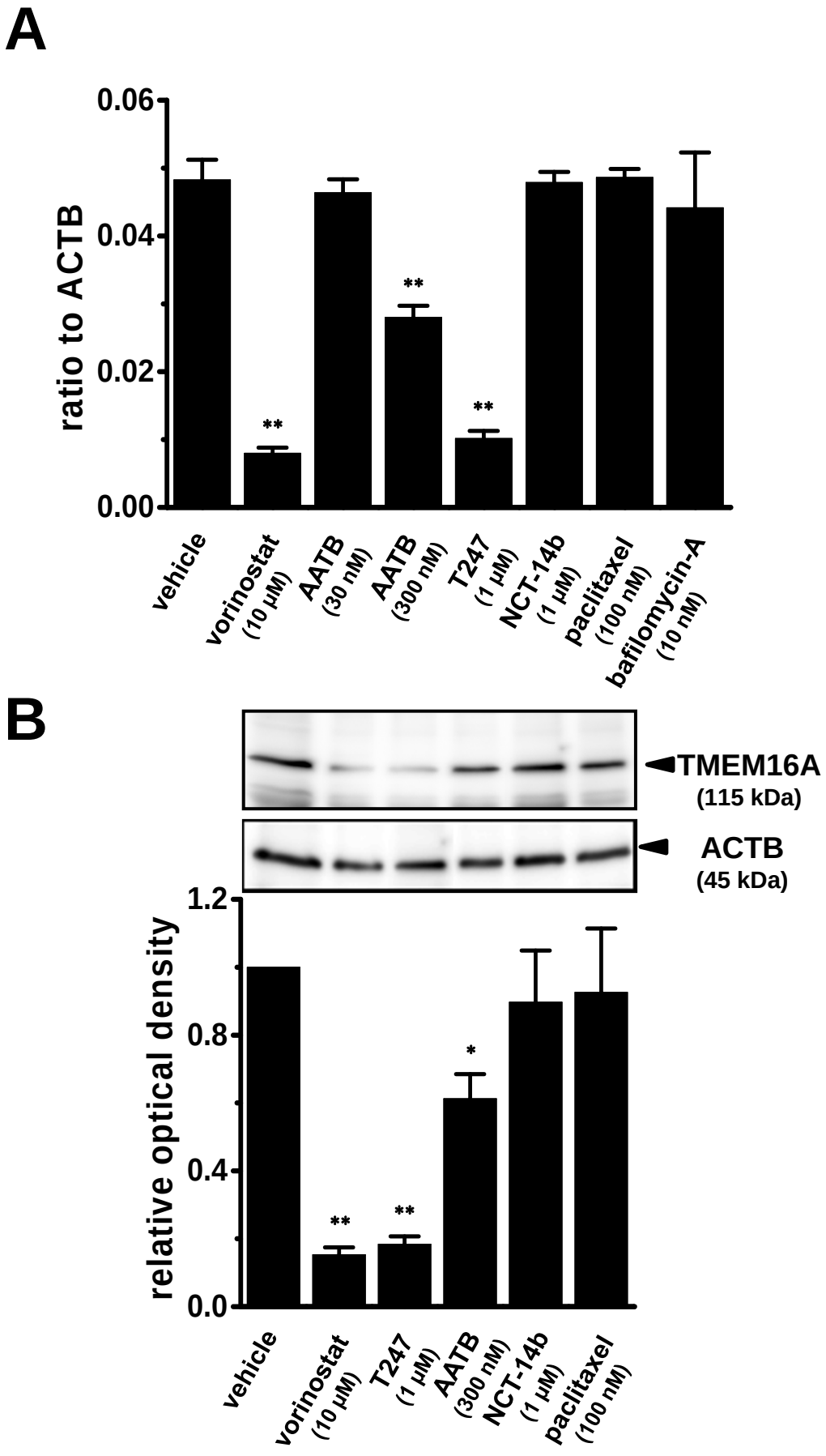

JPET Fast Forward. Published on September 17, 2014 as DOI: 10.1124/jpet.114.217315
This article has not been copyedited and formatted. The final version may differ from this version.

Fig. 4

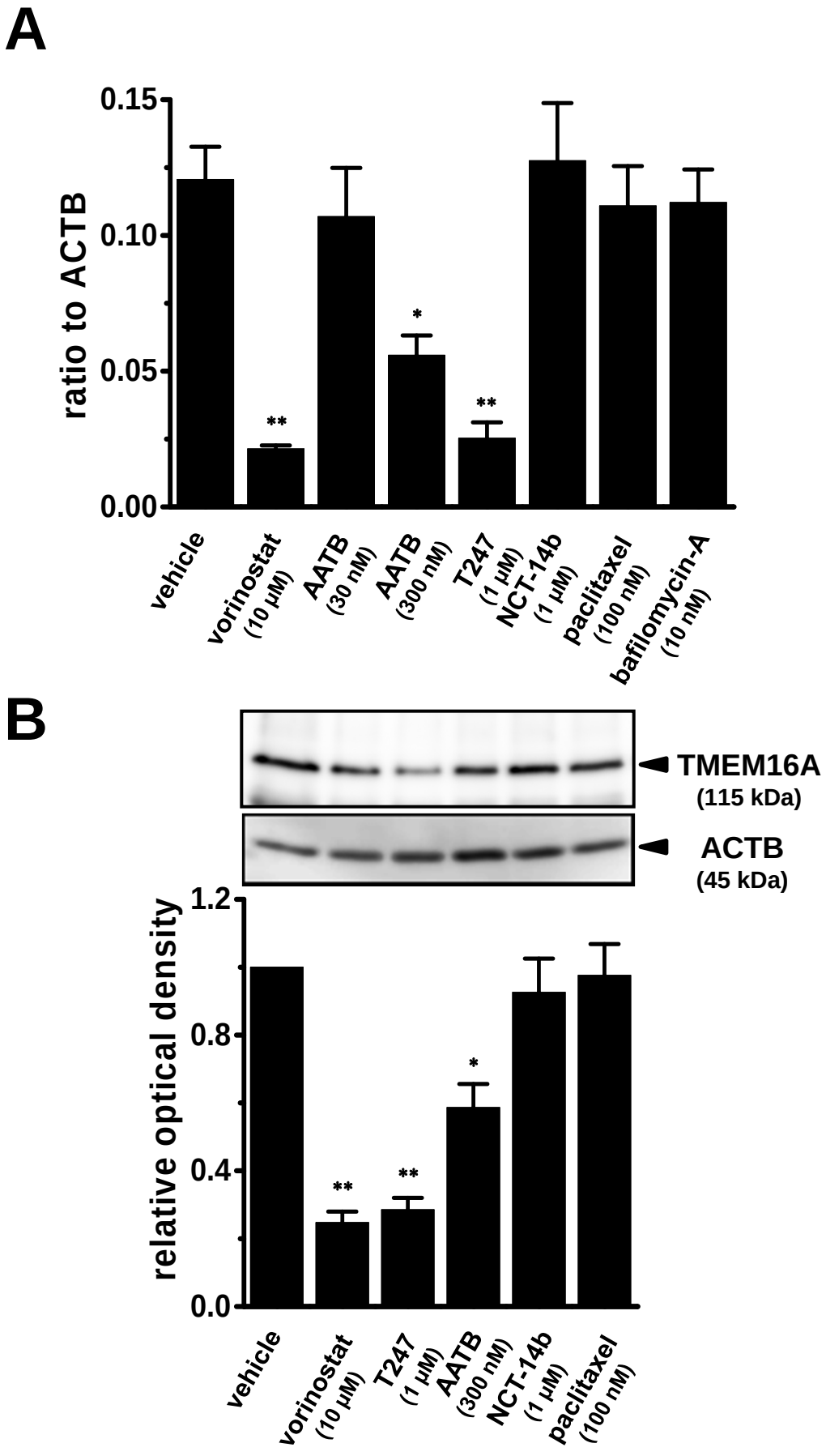

JPET Fast Forward. Published on September 17, 2014 as DOI: 10.1124/jpet.114.217315
This article has not been copyedited and formatted. The final version may differ from this version.

Fig. 5

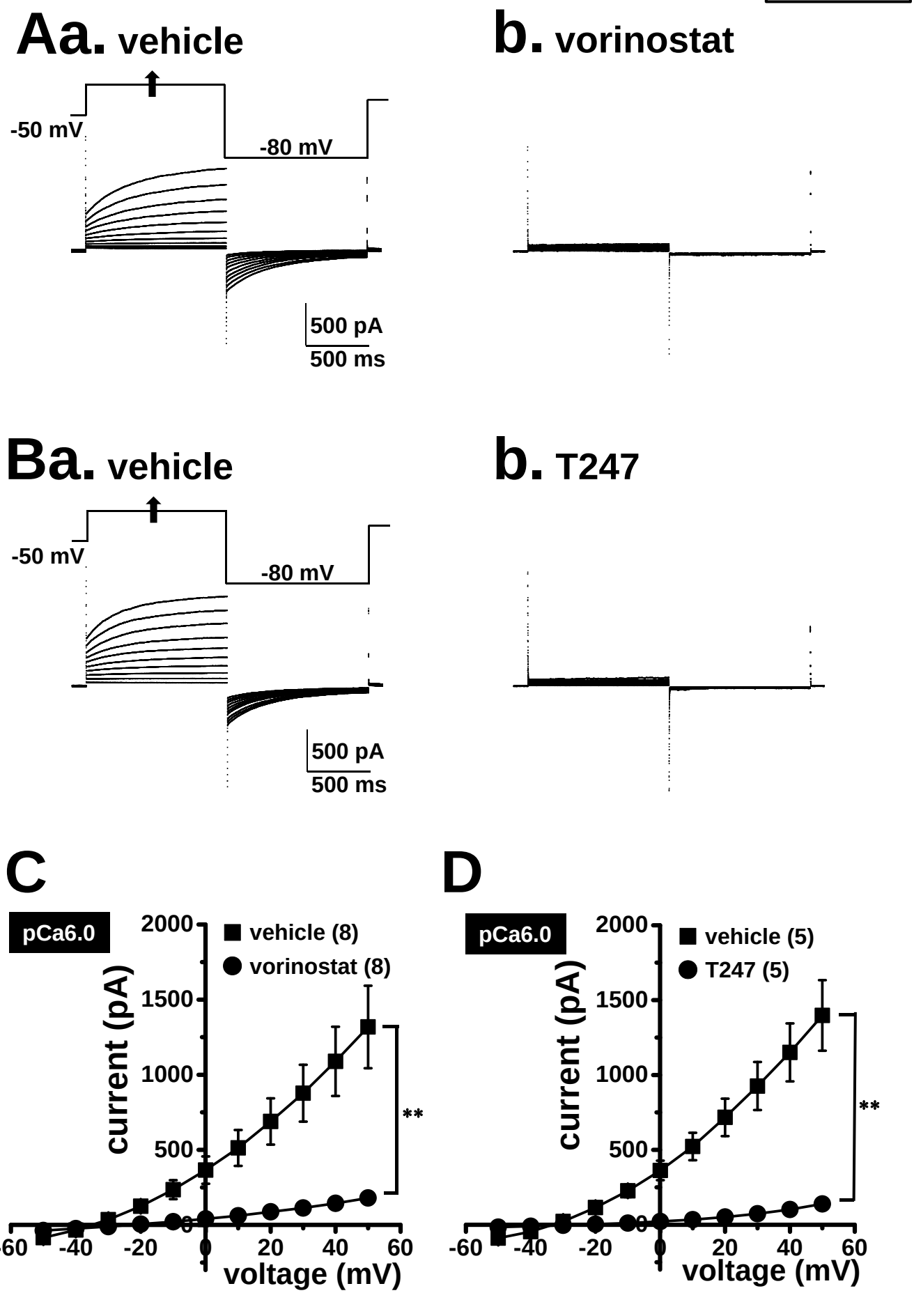

JPET Fast Forward. Published on September 17, 2014 as DOI: 10.1124/jpet.114.217315
This article has not been copyedited and formatted. The final version may differ from this version.

Fig. 6

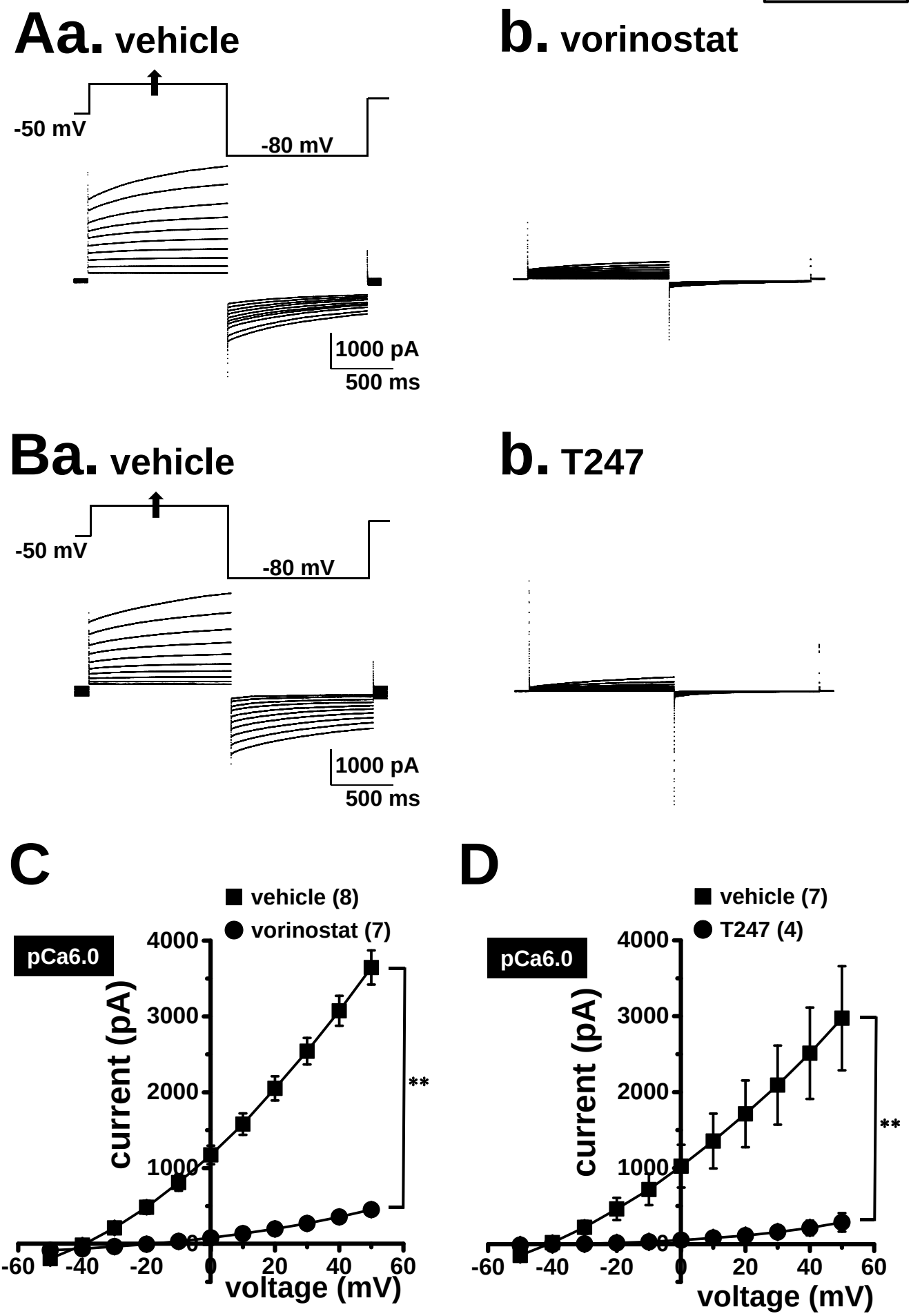

JPET Fast Forward. Published on September 17, 2014 as DOI: 10.1124/jpet.114.217315

Fig. 7

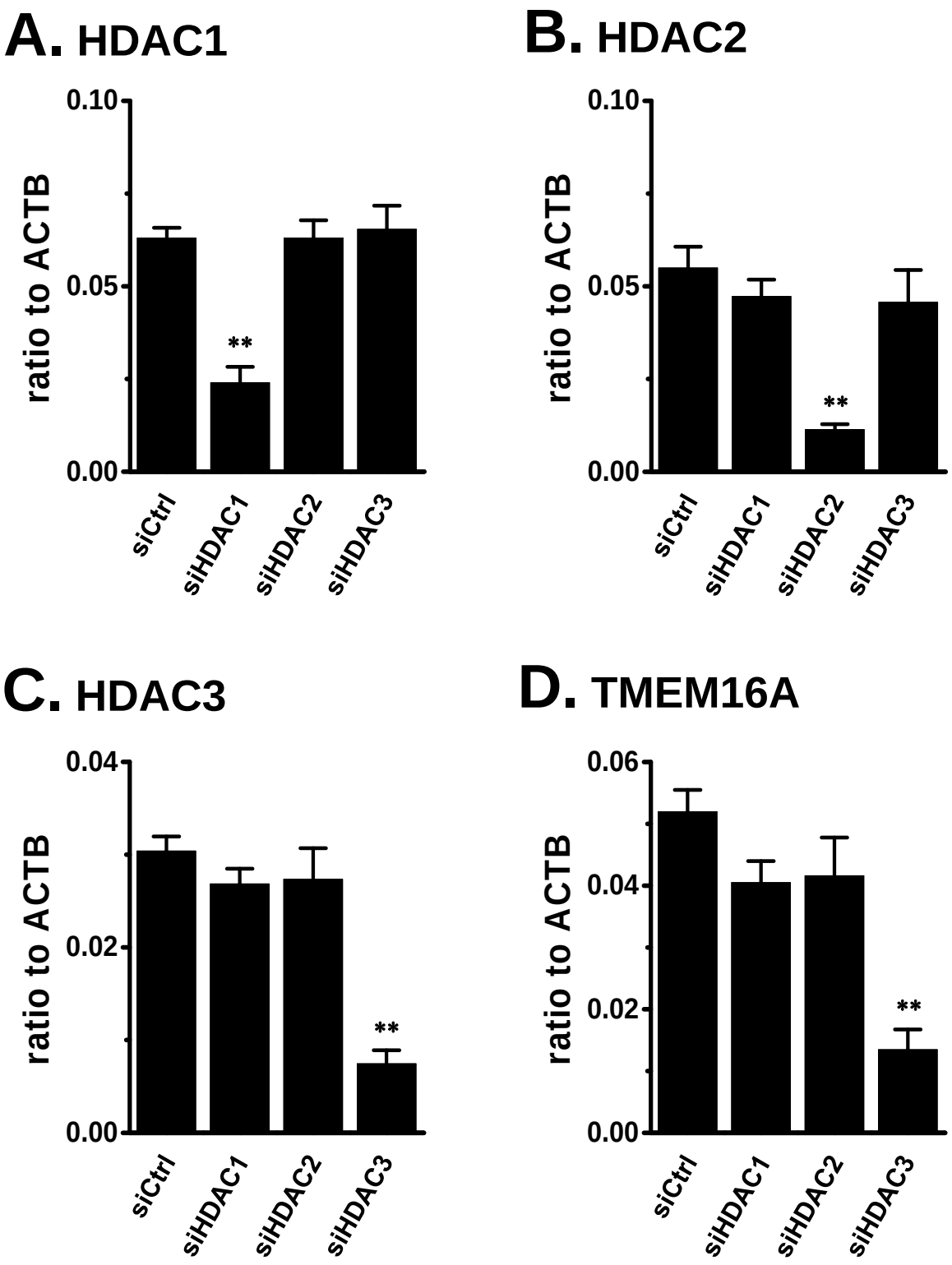

JPET Fast Forward. Published on September 17, 2014 as DOI: 10.1124/jpet.114.217315

Fig. 8